Time-Resolved Magnetic Resonance Fingerprinting for Radiotherapy Motion Management

Tian Li[1][*][†], MSc, Di Cui[2][*], PhD, Edward S. Hui[2], PhD, Jing Cai[1], PhD

1 Department of Health Technology and Informatics, The Hong Kong Polytechnic University, Hong Kong;

2 Department of Diagnostic Radiology, The University of Hong Kong, Hong Kong.

* The two authors contributed equally to this work

† This author is responsible for statistical analyses

Co-corresponding Authors:

Jing Cai, PhD

Associate Professor
Department of Health Technology and Informatics
The Hong Kong Polytechnic University
Tel: (852) 3400 8645
Fax: (852) 2362 4365

Edward S. Hui, PhD

Research Assistant Professor
Department of Diagnostic Radiology
The University of Hong Kong
Tel: (852) 2831 5012
Fax: (852) 2817 4013

Short Title: Feasibility Study of Time-Resolved MRF

1 **Abstract**

2 **Purpose:** This study aims to develop a novel time-resolved magnetic resonance

3 fingerprinting (TR-MRF) technique for respiratory motion imaging applications.

4 **Methods and Materials:** The TR-MRF technique consists of repeated MRF

5 acquisitions using an unbalanced steady-state free precession sequence with spiral-in-

6 spiral-out trajectory. TR-MRF was first tested via computer simulation using a 4D

7 extended cardiac-torso (XCAT) phantom for both regular and irregular breathing

8 profiles, and was tested in three healthy volunteers. Parametric MRF maps at different

9 respiratory phases were subsequently estimated using our TR-MRF sorting and

10 reconstruction techniques. The resulting TR-MRF maps were evaluated using a set of

11 metrices related to radiotherapy applications, including absolute difference in motion

12 amplitude, error in the amplitude of diaphragm motion (ADM), tumor volume error

13 (TVE), signal-to-noise ratio (SNR), and tumor contrast.

14 **Results:** TR-MRF maps with regular and irregular breathing were successfully

15 generated in XCAT phantom. Numerical simulations showed that the TVE were 1.6±2.7%

16 and 1.3±2.2%, the average absolute differences in tumor motion amplitude were

17 0.3±0.7 mm and 0.3±0.6 mm ,and the ADM were 4.1±0.9% and 3.5±0.9% for irregular

18 and regular breathing respectively. The SNR of the T_1 and T_2 maps of the liver and the

19 tumor were generally higher for regular breathing compared to irregular breathing,

20 whereas tumor-to-liver contrast is similar between the two breathing patterns. The

21 proposed technique was successfully implemented on the healthy volunteers.

22   **Conclusion:** We have successfully demonstrated in both digital phantom and health

23   subjects a novel TR-MRF technique capable of imaging respiratory motions with

24   simultaneous quantification of MR multi-parametric maps.

1. Introduction

Tumor motion imaging is of vital importance in managing mobile cancers in radiation therapy. Inadequate motion management could lead to treatment margins that over-irradiate healthy tissues or under-irradiate the target. To address this issue, four-dimensional (4D) imaging techniques[1,2] have been developed to quantify respiratory motions, which are quasi-periodic and patient specific.[3] Typically, 4D techniques entail two (2D) or three-dimensional (3D) imaging of anatomy over several respiratory cycles, and concurrent record of either internal or external respiration signal or surrogate.[4-6] MRI is an ideal alternative to most widely used 4D computed tomography (4D-CT) due to its exquisite soft-tissue contrast and zero ionizing radiation.[2] There are two broad categories of MRI methods for motion tracking: real-time acquisition[7] and retrospective reconstruction.[8,9] The former has limited spatial resolutions with current MRI capacity whilst the latter can be confounded by irregular breathing.[2] As retrospective reconstruction has significantly lower requirements on scanner hardware and computing resources, it has largely been the method of choice.[10]

The keys to the reconstruction of time-resolved respiratory motions using retrospective MRI methods relate to the temporal resolution of MRI acquisition and how the raw MRI data from different respiratory phases and cycles are sorted and combined. An optimal motion tracking technique should thus have good spatiotemporal resolution and a robust algorithm for retrospective reconstruction. We hypothesize that the recently proposed magnetic resonance fingerprinting (MRF) technique could potentially fill this gap and provide different tissue properties maps from one single

47 scan.[11] It is a fast pseudorandomized dynamic acquisition that permits reliable

48 quantification of multiple magnetic resonance (MR) parameters, such as T_1, T_2, and

49 proton-density (PD).[11-15] MRF is based on the premise that the MR signal evolution or

50 fingerprint of distinct tissues will be different when acquisition parameters, such as flip

51 angle and repetition time (TR), are pseudorandomized.[11] Recent studies have

52 demonstrated that other biological parameters, including perfusion,[16] diffusion[17] and

53 T_2^* [12] can also be estimated.

54   Considering that MRF permits high spatial and temporal resolutions as well as

55 quantitative imaging, we hypothesize that MRF holds great promises in overcoming the

56 current deficiencies of existing 4D-MRI: inconsistent tumor contrast, inadequate

57 spatiotemporal resolutions and the lack of quantification of tumor response. It is

58 therefore highly desirable to develop 4D-MRF for radiotherapy motion management

59 applications. Nevertheless, MRF is fundamentally different from conventional MRI

60 sequences in data acquisition and image reconstruction, making it intrinsically

61 challenging for motion imaging. In this study, we aim to resolve a key technical problem

62 in the development of 4D-MRF by developing a time-resolved MRF technique (TR-

63 MRF), or a 'cine-mode'[18] MRF, capable of imaging respiratory motions with

64 simultaneous quantification of MR multi-parametric maps. Achieving TR-MRF will be

65 a key step forward in developing 4D-MRF which has great potential to significantly

66 improve the accuracy and work efficiency of treatment for abdominal cancers, as

67 compared to CT and conventional MRI. In this study, we evaluated the fidelity and

68 reliability of our proposed TR-MRF in the estimation of regular and irregular

69   respiratory motions in digital phantom and healthy volunteers.

70   **2. Material and methods**

71   **2.1 Digital human phantom**

72   Extended cardiac-torso (XCAT) digital phantom,[9,10,19,20] a highly detailed whole-

73   body numerical dynamic phantom for medical imaging research, was used in this study

74   for the simulation of regular and irregular breathing motions. The T_1 and T_2 of each

75   organ in the XCAT phantom were set according to ref[21-23] and are shown in Table 1.

76   The maximum diaphragm motion was set to 2.0 cm and 1.2 cm in the cranial-caudal

77   (CC) and anterior-posterior (AP) directions, respectively. A tumor with diameter of 3.0

78   cm was added in the center of liver. Voxel size of the digital phantom is 1.67 mm

79   isotropic. Respiratory period of 4.8 s and frame rate of 12 ms were set for the simulation

80   of regular breathing pattern. For irregular breathing pattern, the respiratory period

81   varies from 3 s to 5 s and the maximum diaphragm motion ranges from 1.0 cm to 2.0

82   cm.

83

84   **2.2 Simulation of TR-MRF acquisition**

85   MRF acquisition with an inversion-recovery unbalanced steady-state free

86   precession sequence[24] was simulated using the extended phase graph algorithm.[25] It

87   was assumed that the tissue was static within each time points in the creation of

88   dictionary and in the simulation. Regular and irregular breathing, as shown in Figure 2

89   (E) and (F), during MRF acquisition were simulated. A variable density spiral-in-spiral-

90 out readout trajectory with acquisition window of 8.4 ms and acceleration factor = 58.4

91 was used. The trajectory was rotated by a golden angle of 222.5° after each dynamic.

92 The acquisition matrix = 256 x 256, image resolution = 1.17 x 1.17 mm^2, slice thickness

93 = 5 mm. The pseudorandomized FA varied from 0 to 60 degrees and TR varied from 12

94 – 14.25 ms, number of time points (M) = 1000, the acquisition time of a single slice for

95 a single MRF block is 12 -14.25 s, number of acquisitions (N) = 10 (acquired after

96 every 1000 time points), and 5 seconds were added between the end of one acquisition

97 and the beginning of the next to allow for signal recovery. Each MRF block of M time

98 points was triggered by different respiratory phases. The MRF images were simulated

99 for 15 slices in the sagittal direction covering the whole tumor and 1 slice in axial and

100 coronal directions to show efficacy.

101 **2.3 Retrospective MRF reconstruction**

102 The image reconstructed from k-space acquired at a given TR of a MRF block is

103 denoted as dubbed MRF snapshots from hereon. MRF snapshots not only differ in

104 signal intensity but also in spatial content in the presence of motion. In other words,

105 they are no longer the snapshots of the organs in the same location but rather snapshots

106 of the organs at different respiratory phases. As such, the conventional dictionary

107 matching algorithm[11] will no longer work and will produce erroneous parametric maps.

108 Considering that the respiratory phases of the digital phantom is known, we can

109 retrospectively identify the respiratory phase to which each MRF snapshot corresponds.

110 Upon defining the number of bins in a respiratory cycle, the MRF snapshots that fall

111 into a given respiratory bin can be determined. As a result, different groups of MRF

snapshots will be used for the estimation of the MR parametric maps at different respiratory bins. Due to the fact that abdominal organs are constantly moving during MRF acquisition, the number of MRF snapshots suitable for the estimation of the MR parametric maps for a given respiratory bin resolution will be substantially smaller than the number of acquired time points per MRF acquisition block. Nine additional MRF blocks were thus acquired to ensure that sufficient number of snapshots that fall within a given respiratory bin would be acquired. To obtain the MR parametric maps for all respiratory bins, dictionary matching will be performed using the MRF snapshots that fall within the corresponding respiratory bin. For both regular and irregular breathing, all MRF data was retrospectively sorted into 10 respiratory bins using the phase sorting method. The overall workflow of our proposed retrospective reconstruction is illustrated in Figure 1.

The fidelity of dictionary matching depends not only on the number of TR's acquired in conventional MRF,[24] but also on the number of MRF snapshots that fall within a given respiratory bin for TR-MRF. In other words, there exists a trade-off between dictionary matching fidelity and respiratory bin resolution (i.e. higher bin resolution translates to lower dictionary matching fidelity for patients with regular breathing). For patient with irregular breathing, the number of MRF time points available for a given respiratory bin decreases as compared to patient with regular breathing.

2.4 Analysis of the fidelity of dictionary matching

The fidelity of the dynamic MR parametric maps reconstructed from our proposed

TR-MRF method was evaluated using their absolute values, signal-to-noise-ratio (SNR), tumor contrast, absolute difference in motion amplitude, error in the amplitude of diaphragm motion (ADM) and tumor volume error (TVE). The ADM is defined as:

$$\text{ADM} = \left| \frac{\text{Motion}_{\text{TR\_MRF}} - \text{Motion}_{\text{4D\_XCAT}}}{\text{Motion}_{\text{4D\_XCAT}}} \right| \times 100\%,$$

where $\text{Motion}_{\text{TR-MRF}}$ and $\text{Motion}_{\text{4D-XCAT}}$ are the maximum diaphragm motion amplitude between end of inhalation (EOI) and end of exhalation (EOE) measured from MR parametric maps and the digital phantom, respectively. The TVE is defined as:

$$\text{TVE} = \left| \frac{\text{Volume}_{\text{TR\_MRF}} - \text{Volume}_{\text{4D\_XCAT}}}{\text{Volume}_{\text{4D\_XCAT}}} \right| \times 100\%,$$

where $\text{Volume}_{\text{MRMRF}}$ and $\text{Volume}_{\text{4DXCAT}}$ are the contoured tumor volume measured from MR parametric maps and the digital phantom, respectively. The tumor volumes were contoured from MR parametric maps and digital phantom over 10 respiratory phases. The absolute T_1 and T_2 values, DMAE and TVE measured from the digital phantom are considered as gold standard. All measurements were conducted in all 10 respiratory phases across the 15 sagittal slices and were expressed as mean ± standard deviation.

2.5 Volunteer study

Three healthy volunteers were recruited to test the feasibility of our proposed method. MRI was performed using 3.0 Tesla human MRI scanner (Achieva TX, Philips Healthcare) with 8-channel torso coil for signal reception. Acquisition scheme and all imaging parameters were the same as those described in Section 2.2. The acquisition time of a single slice for a single MRF block and entire TR-MRF acquisition were 13.2 seconds and 3.0 minutes, respectively. Multi-slice imaging was performed using sequential scanning of TR-MRF in different slice locations. The number of slices

acquired were 1 to 3 slices in the sagittal plane for different volunteers, corresponding

to total scan time of 3.0 to 9.1 minutes. Respiratory signals were recorded using

respiratory bellows for retrospective reconstruction.

3. Results

Time-resolved MRF was successfully simulated and tested on volunteer data. The

reconstruction time for one slice is 2.5 minutes. The T_1 and T_2 maps of 10 respiratory

phases in the presence of irregular (A and C) and regular (B and D) breathing are shown

in Figure 2. The T_1 map of 10 respiratory phases in the presence of irregular breathing

are shown in Figure 3. Those obtained from our proposed TR-MRF method across three

planes are shown in Figures 3A to 3C, and those from the gold standard along the

sagittal plane in Figure 3D. The measured motion trajectories in CC and AP directions

for both irregular breathing (G) and regular breathing (H) are shown in Figure 2. The

average absolute difference in motion amplitude are 0.3 ± 0.7 mm and 0.3 ± 0.6 mm

for irregular and regular breathing, respectively. The ADM are $4.1\% \pm 0.9\%$ and 3.5%

$\pm 0.9\%$ for irregular and regular breathing, respectively. The TVE are $1.8\% \pm 2.9\%$ and

$1.3\% \pm 2.2\%$ for irregular and regular breathing, respectively.

The average percentage errors of T_1 and T_2, SNR and tumor contrast results in the

presence of irregular and regular breathing are shown in Table 2. The MRF acquisition

on XCAT without motion was used as baseline and the results of image quality

assessment are also shown in Table 2.

T_1, T_2, and PD maps of a representative volunteer are shown in Figure 4. The

178   average and standard deviation of the breathing cycle was 3.7 ± 0.9 s. T_1-weighted, PD-

179   weighted and T_2-weighted images estimated from MR parametric maps are shown in

180   Figure 5. The average T_1 and T_2 values of liver were 758.9 ± 35.0 ms and 51.0 ± 9.7

181   ms, respectively. The average T_1 and T_2 values of renal cortex were 1267.9 ± 67.9 ms

182   and 63.0 ± 7.4 ms, respectively. The average SNR of the T_1 and T_2 maps for liver are

183   9.0 ± 1.7 and 3.0 ± 0.7, respectively.

184   **4. Discussion**

185   Imaging has recently led to two paradigm shifts in radiotherapy in a hope to improve

186   treatment efficacy, namely voxelization paradigm - the use of a nonuniform dose

187   distribution that depends on the intratumural heterogeneity, and adaptation paradigm –

188   detection and quantification of tissue changes during treatment with imaging.[1]

189   Altogether, the diagnostic value of and the accuracy in the estimation of tumor motion

190   using imaging are pivotal to the reduction of uncertainties in and to the efficacy of

191   radiotherapy. Current 4D MRI techniques can only provide one type of weighted

192   images for one scan, typically T_1-weighted or T_2-weighted[10,26]. However, different

193   types of tumors may be better visualized using different weighted images. It is thus

194   imperative that a better alternative to existing MRI methods for the estimation of motion

195   be developed. Unlike conventional MRI, MRF allows for the simultaneous

196   quantification of multiple tissue properties (T_1, T_2, proton-density, etc.) in a single,

197   time-efficient acquisition. MRF has great potential to significantly improve the

198   accuracy and work efficiency of treatment for abdominal cancers, as compared to CT

199   and conventional MRI. This gap may potentially be addressed by the 4D-MRF

200   technique. In this study, we have successfully demonstrated a novel TR-MRF

201   techniques by developing novel sorting and reconstruction methods uniquely tailored

202   for MRF. The TR-MRF technique can image the respiratory motion and simultaneously

203   quantify multiple MR parameters, a critical step towards the development of 4D-MRF.

204   Overall, the respiratory motions obtained from our proposed TR-MRF method in

205   the presence of regular breathing have better image quality than irregular breathing.

206   The primary reason may pertain to the higher number of MRF snapshots available for

207   the retrospective reconstruction of a given respiratory phase in the presence of regular

208   breathing, whilst irregular breathing rendered fewer number of MRF snapshots suitable

209   for dictionary matching of a given respiratory bin. Nonetheless, both cases showed

210   comparable motion measurement as compared to prior studies[6,10,27], indicating the high

211   fidelity of our proposed TR-MRF method. Compared to the non-moving baseline MRF

212   images, more respiratory phases (less intra-phase motion) and greater oversampling

213   will be helpful to improve T_1 and T_2 accuracy. However, this will require longer

214   scanning time to obtain enough data. Further investigation is warranted to improve the

215   T_1 and T_2 accuracy. From the volunteer study, the liver-lung boundary can be clearly

216   identified in the acquired MRF maps. The vessels in the liver and the internal structure

217   of the kidney are also clearly demonstrated in the maps. The measured T_1 and T_2 values

218   for liver and renal cortex in volunteers are in good agreement comparing to the value

219   reported before, indicating the fidelity of our proposed technique. The noise in the lung

220   compromised lung detail and the T_2 maps show inferior quality than T_1 maps. Although

most of the noise is removed by post-processing, there is still some in the lung and the

liver-lung boundary. The retrospective estimation of contrast-weighted images from

MR parametric maps (e.g. Figure 5) could be potentially used to differentiate various

organs and target of interest. It is noteworthy that 10 acquisitions of MRF block were

performed in the current implementation of TR-MRF under the assumption that there

would be adequate number of MRF snapshots for retrospective dictionary matching for

regular breathing. We will investigate in future studies whether the fidelity of

retrospective dictionary matching for the case of irregular breathing could be improved

by acquiring more MRF blocks.

Further studies are warranted to develop 4D-MRF technique by applying our

proposed TR-MRF method either by multi-slice imaging technique or by volumetric

MRF technique. Another aspect of this technique to be improved is to reduce the image

acquisition time of TR-MRF. The original MRF method[11], as implemented in this study,

is a single-slice acquisition technique. The acquisition time of our current TR-MRF

implementation for the estimation of the MR parametric maps for 10 respiratory phases

of a single slice is 3.0 minutes. For multi-slice imaging, the scan time will increase with

the number of imaging slices, rendering TR-MRF significantly longer than

conventional 4D-MRI imaging, which is typically under 10 minutes.[28,29] To accelerate

multi-slice imaging, multiband technology[30,31] can be used to increase the acquisition

efficiency of TR-MRF by at least a factor of three.[32] Another strategy is to reduce the

number of MRF time points to further improve the acquisition efficiency (by ~60%) at

the slight cost of reducing the fidelity of dictionary matching (e.g. up to 17% error in

243   T$_2$, data not shown). Alternatively, volumetric imaging together with parallel imaging

244   and sliding window reconstruction can also be adopted[33-35] so that a single acquisition

245   of MRF block with image resolution of 1 x 1 x 4 mm^3 for a coverage of 240 x 240 x

246   132 mm^3 can be completed in approximately 40 seconds. Furthermore, machine

247   learning has been recently applied to the MRF process to accelerate acquisition and

248   reconstruction.[36] It can achieve faster and more accurate reconstruction with less MRF

249   data efficiency which is of vital importance in TR-MRF technique.

250 **5. Conclusion**

251   We have successfully demonstrated in both digital phantom and health subjects a

252   novel TR-MRF technique capable of imaging respiratory motions with simultaneous

253   quantification of MR multi-parametric maps.

257 **7. Conflict of interest**

258   The authors have no conflict to disclose.

8. References

1. Jaffray DA. Image-guided radiotherapy: from current concept to future perspectives. *Nat Rev Clin Oncol.* 2012;9(12):688-699.

2. Brandner ED, Chetty IJ, Giaddui TG, Xiao Y, Huq MS. Motion management strategies and technical issues associated with stereotactic body radiotherapy of thoracic and upper abdominal tumors: A review from NRG oncology. *Med Phys.* 2017;44(6):2595-2612.

3. Benchetrit G. Breathing pattern in humans: diversity and individuality. *Respiration Physiology.* 2000;122(2-3):7.

4. Keall P. 4-dimensional computed tomography imaging and treatment planning. *Semin Radiat Oncol.* 2004;14(1):81-90.

5. Yang J, Cai J, Wang H, et al. Is diaphragm motion a good surrogate for liver tumor motion? *Int J Radiat Oncol Biol Phys.* 2014;90(4):952-958.

6. Yang J, Cai J, Wang H, et al. Four-dimensional magnetic resonance imaging using axial body area as respiratory surrogate: initial patient results. *Int J Radiat Oncol Biol Phys.* 2014;88(4):907-912.

7. Blackall JM, Ahmad S, Miquel ME, McClelland JR, Landau DB, Hawkes DJ. MRI-based measurements of respiratory motion variability and assessment of imaging strategies for radiotherapy planning. *Phys Med Biol.* 2006;51(17):4147-4169.

8. von Siebenthal M, Szekely G, Gamper U, Boesiger P, Lomax A, Cattin P. 4D MR imaging of respiratory organ motion and its variability. *Phys Med Biol.* 2007;52(6):1547-1564.

9. Liu Y, Yin FF, Chen NK, Chu ML, Cai J. Four dimensional magnetic resonance imaging with retrospective k-space reordering: a feasibility study. *Med Phys.* 2015;42(2):534-541.

10. Cai J, Chang Z, Wang Z, Paul Segars W, Yin FF. Four-dimensional magnetic resonance imaging (4D-MRI) using image-based respiratory surrogate: a feasibility study. *Med Phys.* 2011;38(12):6384-6394.

11. Ma D, Gulani V, Seiberlich N, et al. Magnetic resonance fingerprinting. *Nature.* 2013;495(7440):187-192.

12. Rieger B, Zimmer F, Zapp J, Weingartner S, Schad LR. Magnetic resonance fingerprinting using echo-planar imaging: Joint quantification of T1 and T2 * relaxation times. *Magn Reson Med.* 2017;78(5):1724-1733.

13. Buonincontri G, Biagi L, Retico A, et al. Multi-site repeatability and reproducibility of MR fingerprinting of the healthy brain at 1.5 and 3.0T. *Neuroimage.* 2019;195:362-372.

14. Jiang Y, Ma D, Keenan KE, Stupic KF, Gulani V, Griswold MA. Repeatability of magnetic resonance fingerprinting T1 and T2 estimates assessed using the ISMRM/NIST MRI system phantom. *Magn Reson Med.* 2017;78(4):1452-1457.

15. Buonincontri G, Sawiak SJ. MR fingerprinting with simultaneous B1 estimation. *Magn Reson Med.* 2016;76(4):1127-1135.

16. Su P, Mao D, Liu P, et al. Multiparametric estimation of brain hemodynamics with MR fingerprinting ASL. *Magn Reson Med.* 2017;78(5):1812-1823.

17. Panda A, O'Connor G, Lo WC, et al. Targeted Biopsy Validation of Peripheral Zone Prostate Cancer Characterization With Magnetic Resonance Fingerprinting and Diffusion Mapping. *Invest Radiol.* 2019;54(8):485-493.

18. Liu Y, Yin FF, Rhee D, Cai J. Accuracy of respiratory motion measurement of 4D-MRI: A

comparison between cine and sequential acquisition. *Med Phys.* 2016;43(1):179.

19.   Segars WP, Sturgeon G, Mendonca S, Grimes J, Tsui BMW. 4D XCAT phantom for multimodality imaging research. *Medical Physics.* 2010;37(9):4902-4915.

20.   Panta RK, Segars P, Yin FF, Cai J. Establishing a framework to implement 4D XCAT phantom for 4D radiotherapy research. *J Cancer Res Ther.* 2012;8(4):565-570.

21.   Chen Y, Jiang Y, Pahwa S, et al. MR Fingerprinting for Rapid Quantitative Abdominal Imaging. *Radiology.* 2016;279:9.

22.   Chow AM, Gao DS, Fan SJ, et al. Measurement of liver T(1) and T(2) relaxation times in an experimental mouse model of liver fibrosis. *J Magn Reson Imaging.* 2012;36(1):152-158.

23.   Heye T, Yang SR, Bock M, et al. MR relaxometry of the liver: significant elevation of T1 relaxation time in patients with liver cirrhosis. *Eur Radiol.* 2012;22(6):1224-1232.

24.   Jiang Y, Ma D, Seiberlich N, Gulani V, Griswold MA. MR fingerprinting using fast imaging with steady state precession (FISP) with spiral readout. *Magn Reson Med.* 2015;74(6):1621-1631.

25.   Weigel M. Extended phase graphs: dephasing, RF pulses, and echoes - pure and simple. *J Magn Reson Imaging.* 2015;41(2):266-295.

26.   Liu Y, Yin FF, Czito BG, Bashir MR, Cai J. T2-weighted four dimensional magnetic resonance imaging with result-driven phase sorting. *Med Phys.* 2015;42(8):4460-4471.

27.   Yang W, Fan Z, Tuli R, et al. Four-Dimensional Magnetic Resonance Imaging With 3-Dimensional Radial Sampling and Self-Gating-Based K-Space Sorting: Early Clinical Experience on Pancreatic Cancer Patients. *Int J Radiat Oncol Biol Phys.* 2015;93(5):1136-1143.

28.   Deng Z, Pang J, Yang W, et al. Four-dimensional MRI using three-dimensional radial sampling with respiratory self-gating to characterize temporal phase-resolved respiratory motion in the abdomen. *Magn Reson Med.* 2016;75(4):1574-1585.

29.   Cai J, Chang Z, Wang Z, Paul Segars W, Yin FF. Four-dimensional magnetic resonance imaging (4D-MRI) using image-based respiratory surrogate: A feasibility study. *Medical Physics.* 2011;38(12):6384-6394.

30.   Breuer FA, Blaimer M, Heidemann RM, Mueller MF, Griswold MA, Jakob PM. Controlled aliasing in parallel imaging results in higher acceleration (CAIPIRINHA) for multi-slice imaging. *Magn Reson Med.* 2005;53(3):684-691.

31.   Setsompop K, Gagoski BA, Polimeni JR, Witzel T, Wedeen VJ, Wald LL. Blipped-controlled aliasing in parallel imaging for simultaneous multislice echo planar imaging with reduced g-factor penalty. *Magn Reson Med.* 2012;67(5):1210-1224.

32.   Ye H, Cauley SF, Gagoski B, et al. Simultaneous multislice magnetic resonance fingerprinting (SMS-MRF) with direct-spiral slice-GRAPPA (ds-SG) reconstruction. *Magn Reson Med.* 2017;77(5):1966-1974.

33.   Cao X, Liao C, Wang Z, et al. Robust sliding-window reconstruction for Accelerating the acquisition of MR fingerprinting. *Magn Reson Med.* 2017;78(4):1579-1588.

34.   Liao C, Bilgic B, Manhard MK, et al. 3D MR fingerprinting with accelerated stack-of-spirals and hybrid sliding-window and GRAPPA reconstruction. *Neuroimage.* 2017;162:13-22.

35.   Cao X, Ye H, Liao C, Li Q, He H, Zhong J. Fast 3D brain MR fingerprinting based on

multi-axis spiral projection trajectory. *Magn Reson Med.* 2019;82(1):289-301.

36. Fang Z, Chen Y, Liu M, et al. Deep Learning for Fast and Spatially-Constrained Tissue Quantification from Highly-Accelerated Data in Magnetic Resonance Fingerprinting. *IEEE Trans Med Imaging.* 2019.

Table 1. T_1 and T_2 relaxation times of different organs (ref[21-23]) used in the XCAT simulation.

Organs	T_1 (ms)	T_2 (ms)
Liver	750	34
Renal medulla	1600	81
Renal cortex	1200	76
Spleen	1300	61
Muscle	1050	39
Fat	250	68
Tumor	1700	42

Table 2. Image quality assessment of XCAT simulation in T_1 and T_2 maps with irregular and regular breathing.

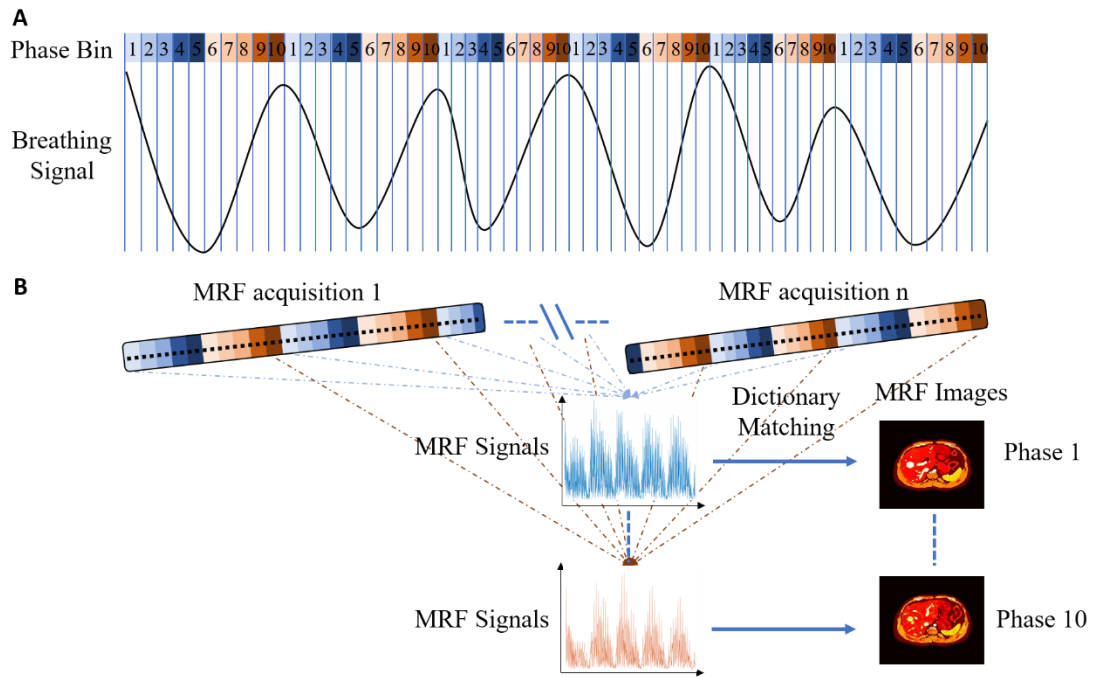|		Irregular breathing	Regular breathing	Baseline
T_1-map	Liver T_1 SNR	7.7 ± 0.7	9.9 ± 0.3	10.3
	Tumor T_1 SNR	6.9 ± 1.9	10.4 ± 0.5	10.7
	Tumor T_1 Contrast	1.7 ± 0.2	1.7 ± 0.1	1.7
	Liver T_1 errors	$13.5 \pm 7.3\ \%$	$10.3 \pm 3.3\ \%$	7.6%
	Tumor T_1 errors	$37.1 \pm 20.7\ \%$	$35.5 \pm 18.2\ \%$	17.7 %
T_2-map	Liver T_2 SNR	4.8 ± 0.8	6.5 ± 0.2	6.6
	Tumor T_2 SNR	2.7 ± 1.4	3.7 ± 2.1	4.5
	Tumor T_2 Contrast	0.3 ± 0.1	0.3 ± 0.1	0.3
	Liver T_2 errors	$8.6 \pm 3.6\ \%$	$7.0 \pm 2.8\ \%$	6.6 %
	Tumor T_2 errors	$11.3 \pm 18.1\ \%$	$10.5 \pm 15.4\ \%$	4.7 %

Figure 1: Illustration of (A) breathing pattern and phase sorting method, and (B) MRF acquisition and reconstruction scheme. Given a breathing pattern, the MRF snapshots that fall into a given respiratory bin can be determined. As such, the estimation of the MR parametric maps for different respiratory bins (different colored bins in A) are obtained from different groups of MRF snapshot.
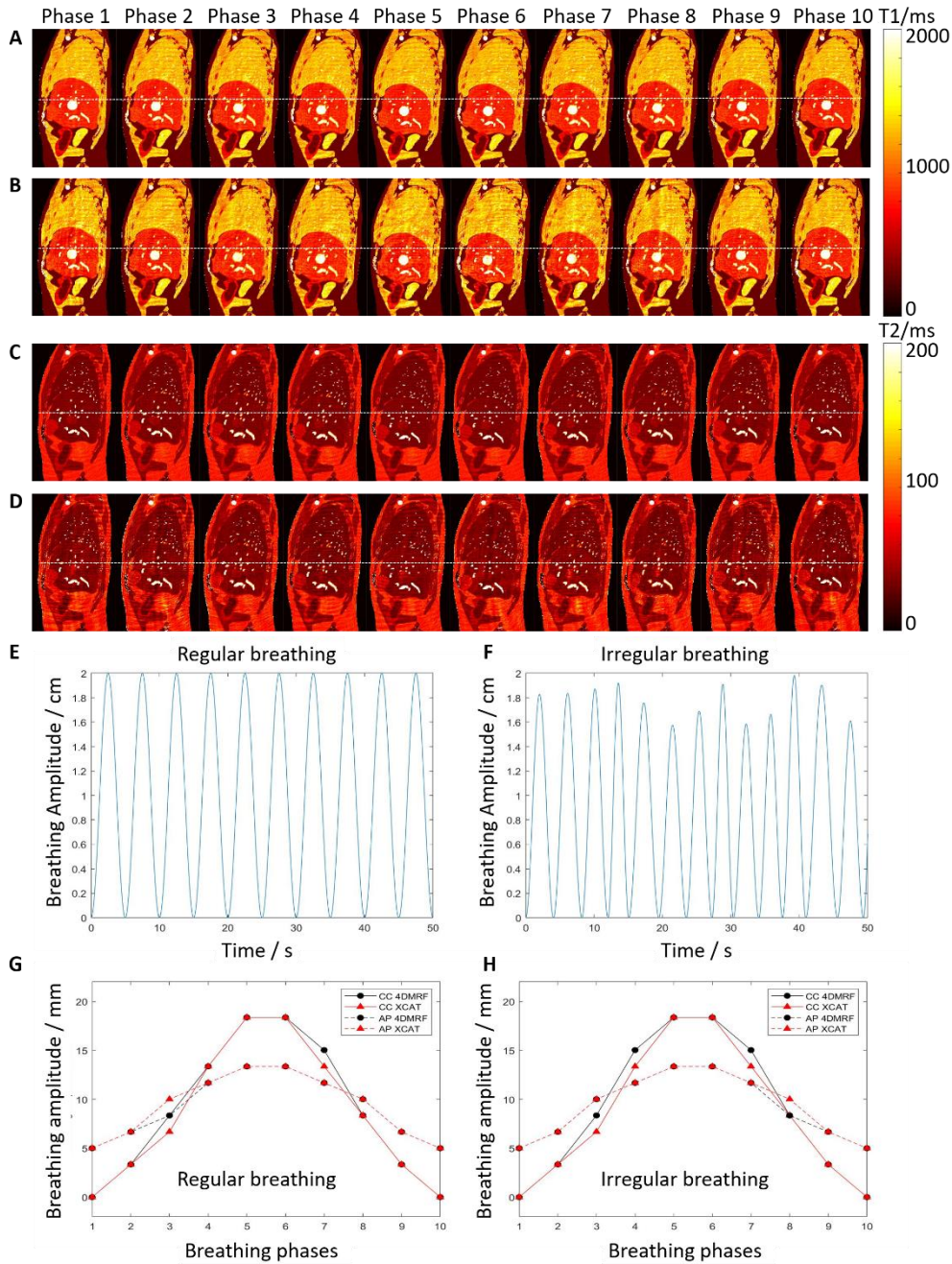
Figure 2: The T_1 (A, B) and T_2 (C, D) maps of the 10 respiratory phases of 4D-MRF reconstructed from XCAT in the presence of regular (A and C) and irregular (B and D) breathing, respectively. Dashed white lines are added to facilitate the visualization of the respiratory motion. Illustration of the regular breathing profile (E) and the irregular breathing profile (F) used in XCAT simulation, as well as the motion trajectories of the pseudo tumor in the CC and AP directions for regular (G) and irregular (H) breathing as measured from T_1 maps of the 10-phase 4D-MRF. The circles denote measurements from 4D-MRF and the rectangles from original 4D-XCAT phantom images as references.
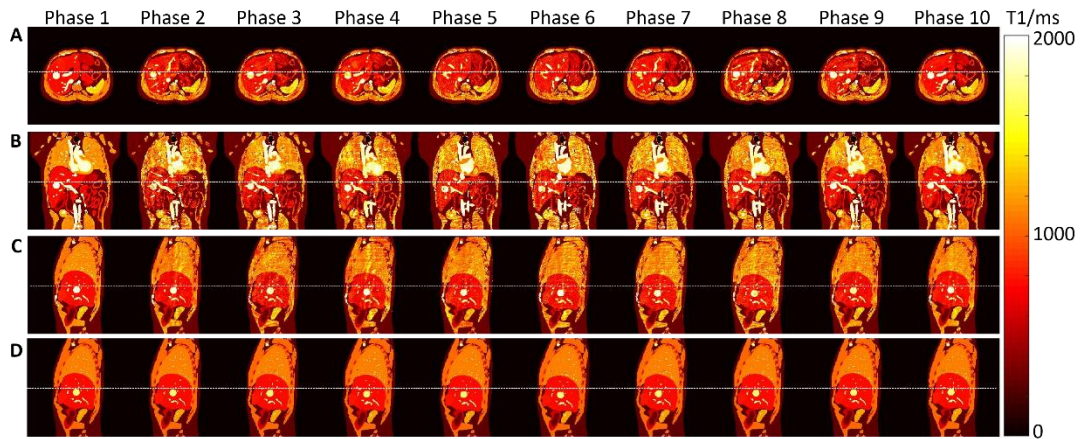
Figure 3: T_1 maps of the 10-phase 4D-MRF reconstructed from the XCAT simulation study using irregular breathing in the axial (A), coronal (B), and sagittal (C) views. The 10-phase XCAT T1 maps in the sagittal view (D) were used as references. Dashed white lines are added to facilitate the visualization of the respiratory motion.
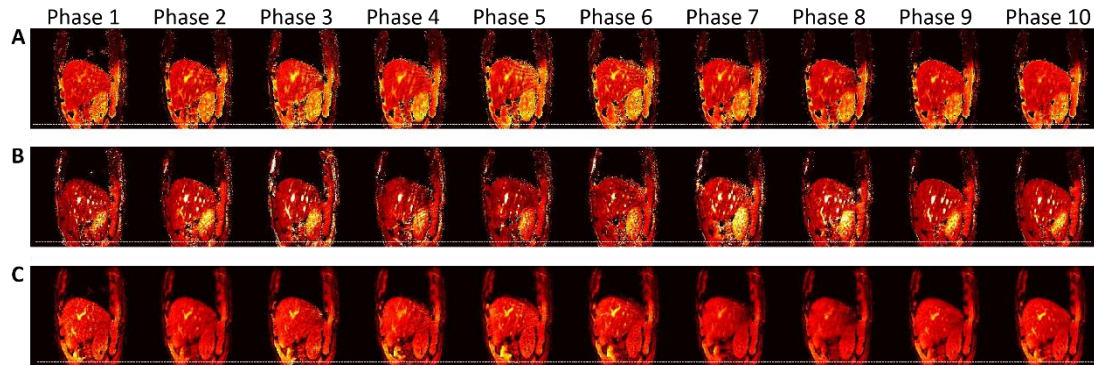

Figure 4: T_1 (A), T_2 (B), and PD (C) maps of 10-phase 4D-MRF images of a representative healthy volunteer. Dashed white lines are added to facilitate the visualization of the respiratory motion.
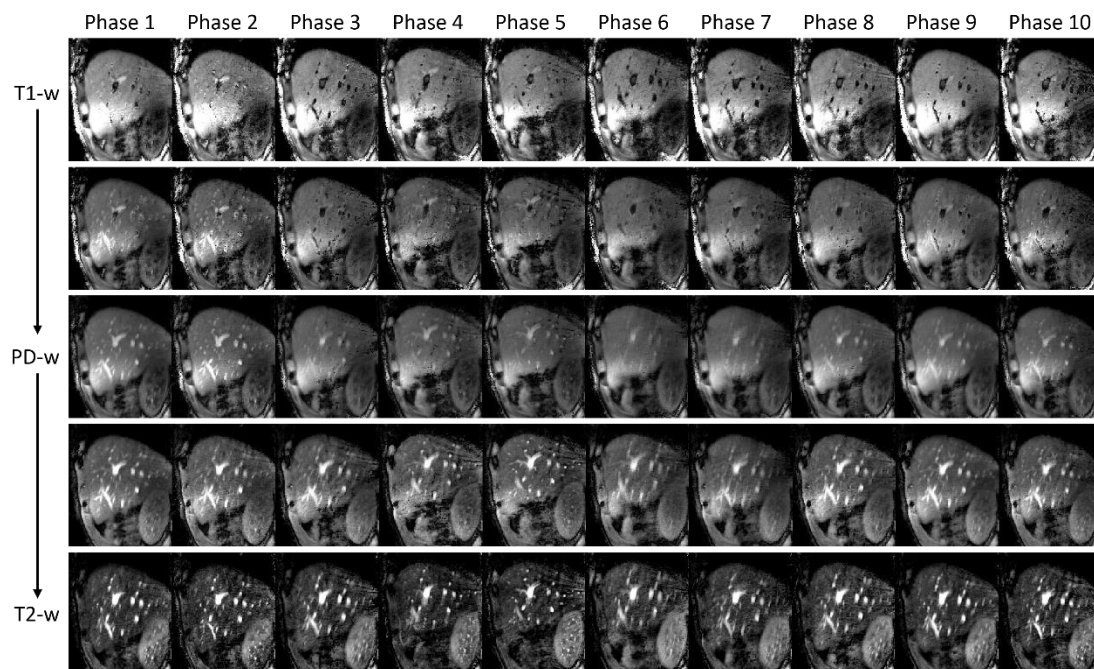
Figure 5: The generated pseudo-contrast 4D MRI images using MRF parameter maps, from T_1-weighted (top) to PD-weighted (middle) and to T_2-weighted (bottom) images.